210. Solution Equilibria in Trialkyl-Phosphite Derivatives of $[Ir_4(CO)_{12}]$. Crystal Structure of $[Ir_4(CO)_{11}\{P(OCH_2)_3CEt\}]$

by **Katya Besançon, Gábor Laurenczy, Tito Lumini,** and **Raymond Roulet***

Institut de Chimie Minérale et Analytique, Université de Lausanne, 3, Place du Château, CH–1005 Lausanne

and **Giuliana Gervasio**

Dipartimento di Chimica Inorganica, Chimica Fisica e Chimica dei Materiali dell'Università, Via Giuria 7, I–10125 Torino

(25.VIII.93)

The monosubstituted $[Ir_4(CO)_{11}L]$ clusters (L = $P(OPh)_3$, **1**; L = $(P(OMe)_3$, **2**; L = $P(OCH_2)_3CEt$, **3**) were obtained in good yields by the reaction of $[Ir_4(CO)_{11}I]^-$ with the corresponding phosphite. In the solid state, cluster **3** has a C_s geometry with all terminal ligands as shown by an X-ray analysis. Three isomers are present in solution: one with terminal ligands (**A**) and two with three edge-bridging CO's and with **L** in axial (**B**) or radial (**C**) position (see *Scheme*). The thermodynamic and kinetic parameters of isomerisations **B**⇄**A** and **A**⇄**C** were determined by simulation of the variable-temperature ^{31}P-NMR spectra. The three isomers correspond to three minima on the kinetic pathway of CO scrambling, whose relative energies vary independently within a small range (1–9 kJ mol^{-1} at 298 K). At low temperature, isomer **C** is always the least stable and is not observed for **1** which bears the most bulky phosphite ligand. The isomerisations are due to two intramolecular merry-go-rounds of CO groups about two unequivalent faces of the unbridged species **A**.

Introduction. – The substitution reactions of $[M_4(CO)_{12}]$ (M = Co, Rh, Ir) by monodentate ligands including trialkyl phosphites were studied in detail [1–7] and were summarised in a textbook [8]. A few studies by multinuclear magnetic resonance appeared, dealing with the structures in solution of $[Rh_4(CO)_{12-x}\{P(OPh)_3\}_x]$ (x = 1–4) and $[Co_4(CO)_{11}\{P(OCH)_3\}]$ and with the fluxional behaviour of $[Rh_4(CO)_8\{P(OPh)_3\}_4]$ [9] [10]. The crystal structures of $[Co_4(CO)_{10}\{P(OCH)_3\}_2]$ and $[Rh_4(CO)_9\{P(OPh)_3\}_3]$ were determined [11] [12]. There is to date no information on the intramolecular dynamics of trialkyl-phosphite derivatives of $[Ir_4(CO)_{12}]$ even though several related studies concerning clusters of the type $[Ir_4(CO)_{11}L]$ appeared (L = PEt_3, PH_2Ph, $PHPh_2$ [13], $PMePh_2$ [2], SO_2, PR_3, Br^-, I^-, NCS^-, NO_2^- [14], H^- [15], t-BuNC [16] [17]). We report here on a thermodynamic and kinetic study of the solution equilibria involving the monosubstituted derivatives of $[Ir_4(CO)_{12}]$ with three different trialkyl phosphites, and on the crystal structure of $[Ir_4(CO)_{11}\{P(OCH_2)_3CEt\}]$.

Solution Equilibria. – The cluster compounds $[Ir_4(CO)_{11}L]$ have a ground-state geometry either with all ligands terminal or with three edge-bridging CO's defining the basal plane of the metal tetrahedron. In the latter case, the ligand L is usually located in axial position. An isomer with L in radial position was observed in solution for L = PEt_3 [13]. Where the ligand L has two bonding modes accessible at moderate energy, it replaces a μ_2-bridging CO, as in $[Ir_4(CO)_9(\mu_2\text{-}CO)_2(\mu_2\text{-}SO_2)]$ [14] or $[Ir_4(CO)_9(\mu_2\text{-}CO)_2(\mu\text{-}H)]^-$ [15] [18], or occupies terminal positions as in $[Ir_4(CO)_{10}H_2)]^{2-}$ [18].

The trialkyl-phosphite derivatives $[Ir_4(CO)_{11}L]$ (L = $P(OPh)_3$, $P(OMe)_3$) were prepared in 15–20% yields and proposed to have a ground-state structure with bridging CO's on the basis of their IR spectra [2]. We now found that the reaction of $(NEt_4)[Ir_4(CO)_{11}I]$ with 1 mol-equiv. of trialkyl phosphite followed by preparative thin-layer chromatography affords $[Ir_4(CO)_{11}L]$ (L = $P(OPh)_3$, **1**; L = $P(OMe)_3$, **2**; L = 4-ethyl-2,6,7-trioxa-1-phosphabicyclo[2.2.2]octane = $P(OCH_2)_3CEt$, **3**) in 62–73% yields. Examination of their variable-temperature IR spectra (example in *Fig. 1*) showed that at least two species are present in solution: an isomer **A** with all ligands terminal and an isomer **B** with edge-bridging CO's. The relative increase in absorbance of the bands typical for μ_2-CO upon raising the temperature indicated that the conversion **1A**→**1B** is endothermic.

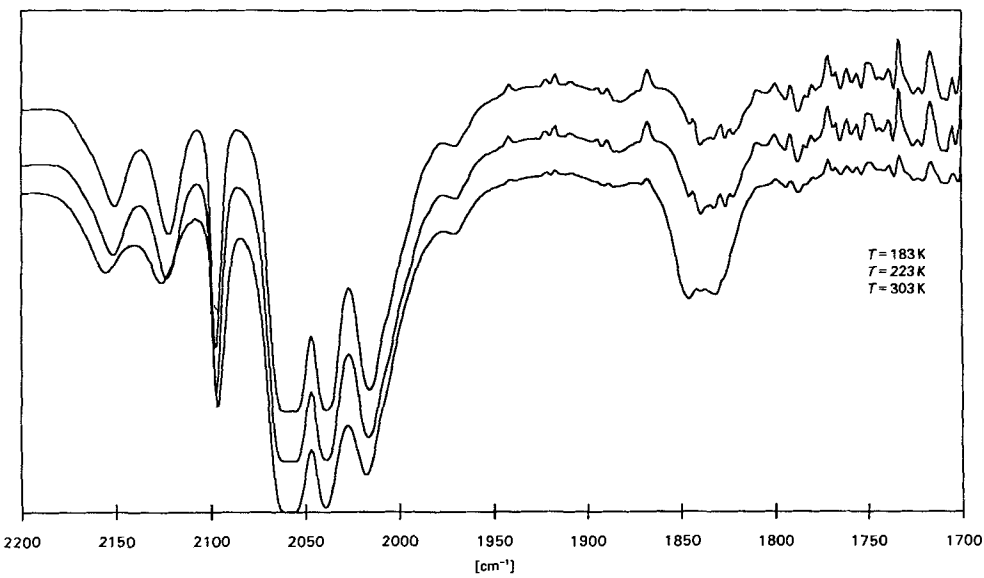

Fig. 1. *Variable-temperature IR spectra of* **1** *in* CH_2Cl_2

The $^{31}P\{^1H\}$-NMR spectrum of **1** in CD_2Cl_2 is blocked at 173 K and presents two resonances with relative intensities 1: 0.03 and with $\Delta\delta$'s(= $\delta_{coord.} - \delta_{free\ L}$) of −10.7 and −31.4 ppm, respectively, the latter value being in the range usually observed for P-donor atoms in axial position [19]. The ^{13}C-NMR spectrum of a sample of **1** enriched in ^{13}CO (*ca.* 30%) is blocked at 173 K and presents two sets of resonances (see *Exper. Part*). A first set can be attributed to the minor isomer **1B** (*ca.* 3%, *Scheme*) and contains two resonances at 202.4 (2 CO) and 195.5 ppm (1 CO) in the range usually observed for edge-bridging CO's [13], two resonances at 170.4 (1 CO) and 169.8 ppm (2 CO) in the range for radial CO's, and one *d* at 150 ppm (1 CO) typical of an apical CO in pseudo-*trans* position relative to a P-atom [13]. The second set of six resonances with relative intensities 2:2:2:2:2:1 has δ's in the range observed for terminal CO's and can confidently be assigned to the major, unbridged isomer **1A**. The geometry of this species is probably similar to that found for the solid state of **3** (see below).

The $^{31}P\{^1H\}$-NMR spectrum of **2** in CD_2Cl_2 is blocked at 173 K and presents three resonances with relative intensities 0.01:0.48:1. A third, minor isomer **2C** (*ca.* 1%) is,

Scheme

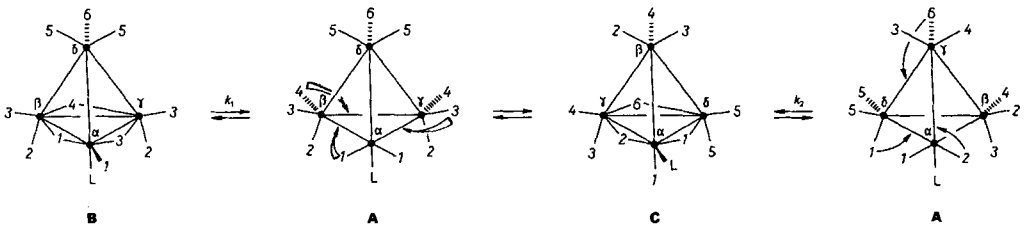

therefore, present in addition to **2A** (32%) and **2B** (67%) (the possibility of **2C** being $[Ir_4(CO)_{10}\{P(OMe)_3\}_2]$ is excluded on the basis of different ^{31}P- and ^{13}C-NMR data). The $\Delta\delta(^{31}P)$ of **2C** relative to **2A** is more positive by *ca.* 35 ppm than that of **2B**. A similar situation was observed by *Mann et al.* [13] for the two isomers of $[Ir_4(CO)_8(\mu_2\text{-}CO)_3(PEt_3)]$ in which the P-atom was found in an axial or radial position. The ^{13}C-NMR spectrum of a sample of **2** enriched in ^{13}CO (*ca.* 30%) is blocked at 173 K and confirms the presence of three isomers (see *Exper. Part*). The major species is the bridged isomer with an axial P-atom (**2B**), since two resonances are observed in the region of edge-bridging CO's (204.2 (2 CO) and 197.0 ppm (1 CO)), two resonances in the region of radial CO's (173.1 (1 CO, $^1J(C,P) = 9$ Hz) and 170.7 ppm (2 CO)), and one *d* in the region of terminal CO's displaying a pseudo-*trans*-C,P coupling. A second set of resonances in the region of terminal CO's with δ's similar to those of **1A** is attributed to the unbridged isomer **2A**. In addition, minor resonances due to **2C** (*ca.* 1%) are observed in the region of bridging CO's and only one resonance (170.8 ppm) in the region of radial CO's with a pseudo-*cis*-C,P coupling ($J \approx 12$ Hz), smaller than pseudo-*trans*-couplings (typically $J = 25$–40 Hz [13] [14]). The remaining resonances are in the region of terminal (axial and apical) CO's. We, therefore, propose **2C** as being the bridged isomer with a $P(OMe)_3$ ligand in radial position.

The ^{31}P- and ^{13}C-NMR spectra of **3** are similar to those of **2**, the corresponding isomers **3A**, **3B**, and **3C** being present in the ratio 0.001:1:0.35 at 173 K.

The variable-temperature $^{31}P\{^1H\}$-NMR spectra of **2** are illustrated in *Fig. 2*. In the slow-exchange domain, the populations p_i of the isomers were determined using the relative integrations of the corresponding resonances. In the fast-exchange region where only one resonance was observed ($\delta_{exp.}$), *Eqns. 1–3* were used to determine the populations and the thermodynamic parameters of the equilibria **B**⇄**A** and **A**⇄**C** (see *Table 1*):

$$\delta_{exp.} = \delta_A p_A + \delta_B p_B + \delta_C p_C \quad (1)$$

$$K_T = \exp(-\Delta H \cdot R^{-1}T^{-1} + \Delta S \cdot R^{-1}) \quad (2)$$

$$p_A = K_1/(1 + K_1 + K_1K_2); \qquad p_B = 1/(1 + K_1 + K_1K_2); \qquad p_C = 1 - p_A - p_B \quad (3)$$

with $K_1 = p_A/p_B$ and $K_2 = p_C/p_A$. In the case of **1**, p_C was set to zero.

The $^{31}P\{^1H\}$-NMR spectra were then used to determine the rate constants of isomerisation. Since only two species are present in the case of **1**, the rate constants k_1 of **1B**→**1A** were calculated from the measured values of the line-widths at half height at different temperatures by fitting the equations describing the generalised relaxation rates as re-

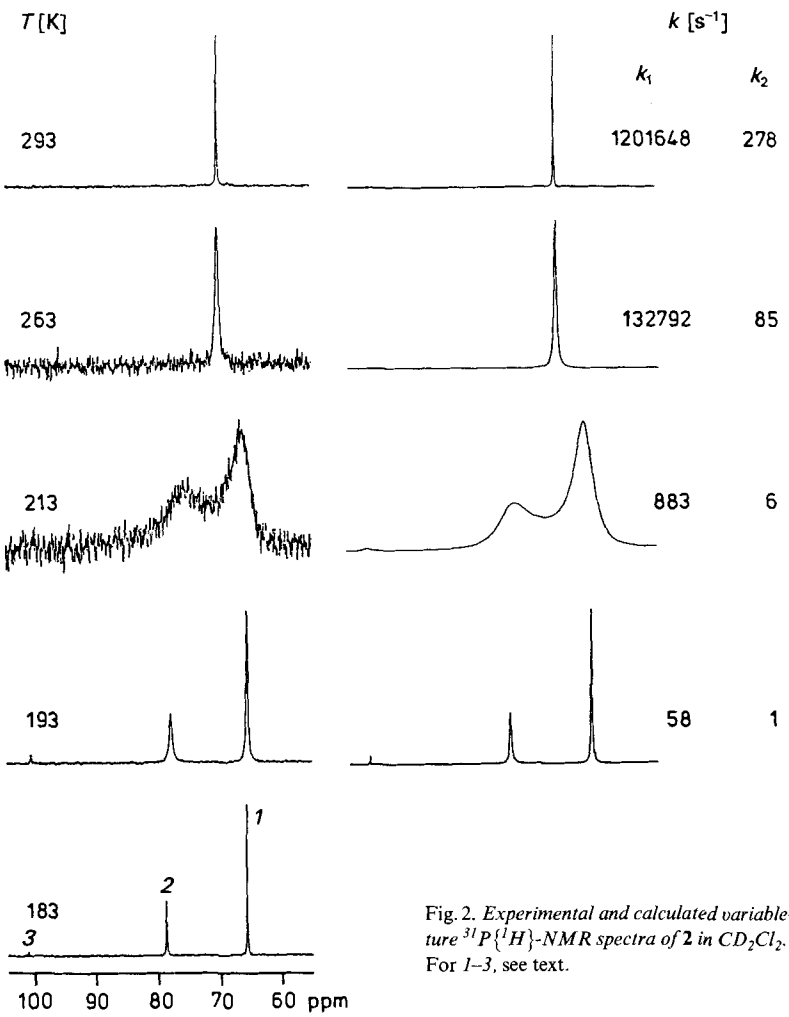

Fig. 2. *Experimental and calculated variable-temperature* $^{31}P\{^1H\}$*-NMR spectra of* **2** *in* CD_2Cl_2. For *1–3*, see text.

ported by *Leigh* [20] (*Fig. 3*). For **2** and **3**, the calculated populations (*Eqns. 1–3*) were introduced in the elements of the following *Kubo-Sack* exchange matrix: $(1,1) = -k_1$, $(1,2) = k_1$, $(2,1) = k_1 p_B/p_A$, $(2,2) = -k_1 p_B/p_A - k_2$, $(2,3) = k_2$, $(3,2) = k_2 p_A/p_C$, and $(3,3) = -k_2 p_A/p_C$ where *1*, *2*, and *3* represent the ^{31}P resonances in order of increasing chemical shift (see *Fig. 2*), and k_1 and k_2 are the rate constants of the exchanges **B**→**A** and **A**→**C**, respectively. Finally, the activation parameters were determined from the graphs $\ln(k/T)$ *vs.* $1/T$ (*Fig. 4*, *Table 1*).

The ^{13}C-NMR spectra of **1–3** are temperature-dependent, and the interconversions between the three isomers are clearly due to CO site exchanges. The most favorable case for study is **1** whose blocked spectrum presents six CO resonances with different chemical shifts for the unbridged, major isomer **1A** (97% at 173 K). Unfortunately, only four CO

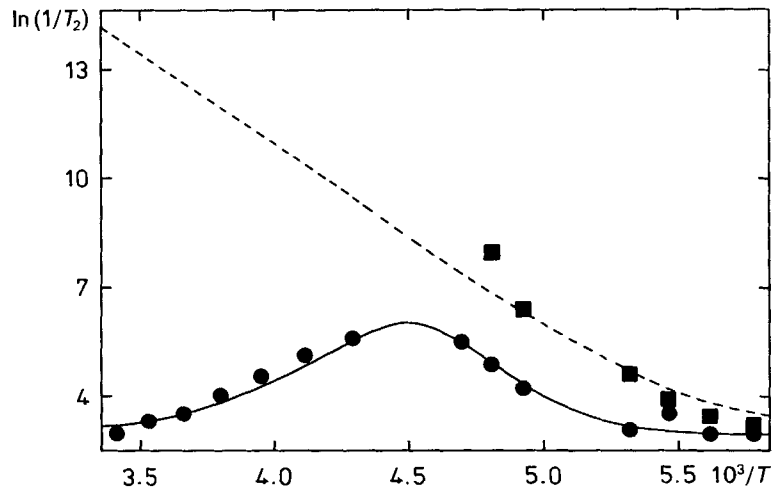

Fig. 3. *Observed transverse relaxation rates for* **1A** *and after coalescence* (●) *and* **1B** (■) *in the slow- and fast-exchange domains*

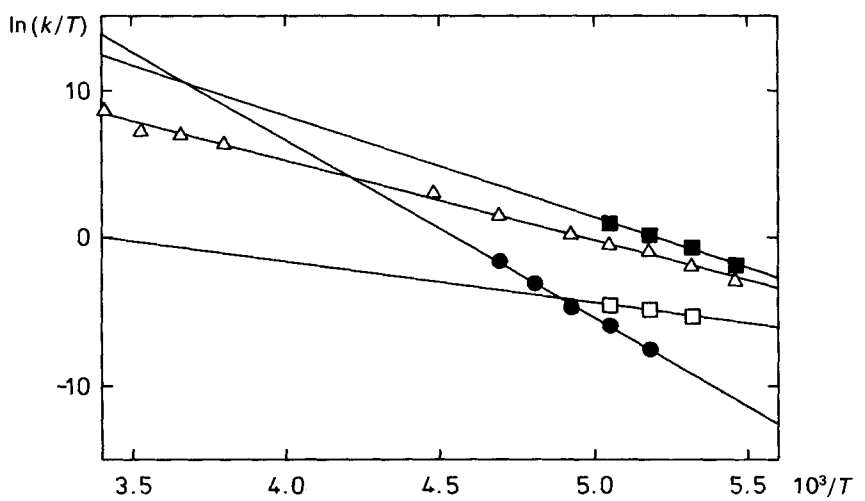

Fig. 4. *Variation of the rate constants of the conversions* **B**→**A** (k_1) *and* **A**→**C** (k_2) *in* CD_2Cl_2 *as function of temperature for* **2** (Δ : k_1; □ : k_2) *and* **3** (■ : k_1; ● : k_2)

resonances of the minor isomer **1B** (corresponding to its bridged and radial CO's) are well separated from those of **1A**, and the relative population of **1B** increases upon raising the temperature. Therefore, the variable-temperature spectra cannot be simulated. However, the dynamic connectivities are ascertained by a COSY spectrum of **1** in CD_2Cl_2 at 188 K and a NOESY spectrum at 193 K (see *Exper. Part*). These are quite similar to those previously observed for $[Ir_4(CO)_{11}(t\text{-BuNC})]$ [17] which has the same C_s geometry as **1A** and for which a quantitative treatment of two NOESY spectra with different mixing

Table 1. *Thermodynamic and Kinetic Parameters for the Solution Equilibria of Trialkyl-Phosphite Clusters* $[Ir_4(CO)_{11}L]$ *at 298 K*

	1 (L = $P(OPh)_3$)	**2** (L = $P(OMe)_3$)	**3** (L = $P(OCH_2)_3CEt$
ΔH_1 [kJ mol^{-1}]	− 14.2 ± 0.1	1.23 ± 0.3	1.87 ± 0.7
ΔS_1 [J mol^{-1} K^{-1}]	− 52.6 ± 4	1 ± 2	18.7 ± 4
K_1	0.52 ± 0.05	0.68 ± 0.05	4.8 ± 0.5
ΔH_2 [kJ mol^{-1}]		− 5.3 ± 1	11.9 ± 2
ΔS_2 [J mol^{-1} K^{-1}]		− 55 ± 19	22 ± 10
K_2	$< 10^{-3}$	0.029 ± 0.003	0.11 ± 0.03
$\Delta G_1^{\neq}$ [kJ mol^{-1}]	39.3 ± 1	37.5 ± 0.4	27.5 ± 2
k_1 [s^{-1}][a])	32 ± 3	112 ± 9	507 ± 30
$\Delta G_2^{\neq}$ [kJ mol^{-1}]		58.6 ± 1	23.4 ± 1.9
k_2 [s^{-1}][a])		2.0 ± 0.1	0.50 ± 0.05

[a]) At 198 K. Extrapolated values of k_1 at 298 K are $7.8 \cdot 10^5$, $1.7 \cdot 10^6$, and $9.4 \cdot 10^7$ s^{-1} for **1**, **2** and **3**, respectively. The corresponding values of k_2 are $3 \cdot 10^2$ and $4.8 \cdot 10^8$ s^{-1} for **2** and **3**, respectively.

times could be achieved. Therefore, we propose that the fluxional behaviour of **1**–**3** is similar to that of the isonitrile cluster, namely that the interconversions **A**⇄**B** and **A**⇄**C** are due to merry-go-round processes of CO groups around the two unequivalent faces of the unbridged isomer containing the Ir-atom linked to the phosphite ligand. These processes are indicated in the *Scheme* by solid arrows for the interconversion **A**⇄**C** and by empty arrows for **A**⇄**B**.

The monosubstituted derivatives of $[Ir_4(CO)_{12}]$ with tertiary phosphines, in particular with the more basic ones, have a ground-state geometry with three edge-bridging CO's probably because the latter are better π-acceptors than terminal CO's. As trialkyl phosphites are better π-acceptors than phosphines, the unbridged isomer **A** can be observed and is even the most stable one below 270 K for L = $P(OPh)_3$. As deduced from the data in *Table 1*, the conversion of **A** to the bridged species **B** and **C** is not always endothermic, and the free enthalpies of the three isomers differ at most by *ca.* 9 kJ mol^{-1} at 298 K. They merely correspond to three relative minima on the graph $\Delta G^{\neq}$ *vs.* reaction coordinate. Isomer **C** (with L in radial position) is not observed for L = $P(OPh)_3$ and is less stable than **B** (with L in axial position) at 298 K for L = $P(OMe)_3$ and $P(OCH_2)_3CEt$ since $\Delta G = -RT\ln(K_1K_2)$ is positive for the conversion **B**→**C**. The same situation was observed for the two bridged isomers of $[Ir_4(CO)_{11}(PEt_3)]$ [13]. The sequence L(axial) < L(radial) for the relative energies of the bridged isomers seems to be followed by all $[Ir_4(CO)_{11}L]$ clusters known to date. This is probably due to the greater steric hindrance of a ligand L more or less coplanar with vicinal μ_2-CO's than that of L in an axial position.

The proposed mechanism for the interconversion **A**→**C** and the observation that the $\Delta G_2^{\neq}$ of process **3A**→**3C** (23 kJ mol^{-1}) is smaller than that of **3A**→**3B** ($\Delta G_1^{\neq} - \Delta G_1 = 31$ kJ mol^{-1}) appears to contradict the fact that a merry-go-round of five CO's was never observed when the ground state of the Ir_4 cluster contains a face bearing a radial ligand L, three edge-bridging, and two terminal CO's [21]. However, in this instance, the ground state has all ligands terminal, and the only condition to be satisfied in the **A**→**C**→**A** process is to finish at a state of equal energy with the same pseudo-*trans* relationship between L and one CO group (*6* in the *Scheme*). This criterion does not place any constraints on the choice of the face for the merry-go-round.

Crystal Structure of $[Ir_4(CO)_{11}\{P(OCH_2)_3CEt\}]$ (3). – The crystal consists of discrete molecules without abnormally close intermolecular contacts. The overall structure of **3** and the labeling scheme are shown in *Fig. 5*. Interatomic distances and angles are collected in *Table 2*.

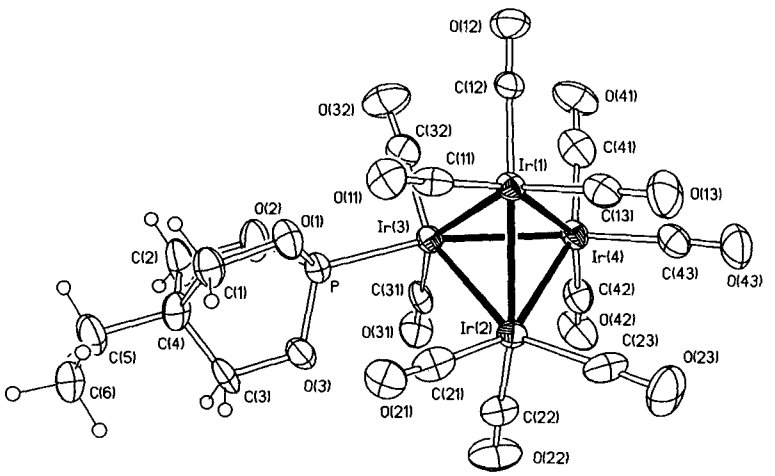

Fig. 5. *ORTEP View of the molecular structure of* **3**. Thermal ellipsoids at 30% probability. Arbitrary numbering.

The molecule contains a nearly tetrahedral Ir_4 core with terminal ligands only: Ir(1), Ir(2), and Ir(4) are linked to three terminal CO's, while Ir(3) is in a unique environment, being linked to two terminal CO's and to a terminal phosphite ligand. The range of Ir–Ir bond distances is wide (2.684(1) to 2.701(1) Å with a difference of 17σ); however, the mean value of the distances involving the unique Ir(3) atom and the average value of the remaining Ir–Ir distances are equal (2.691(1) Å). This molecule is one of the few examples of monosubstituted $[Ir_4(CO)_{11}L]$ clusters devoid of bridging CO's [22]. The phosphite

Table 2. *Bond Lengths* [Å] *and Angles* [°] *for* **3**. For numbering, see *Fig. 5*.

Ir(1)–Ir(2)	2.684 (1)	C(32)–O(32)	1.127 (26)	Ir(4)–C(43)	1.903 (20)
Ir(1)–Ir(4)	2.692 (1)	C(42)–O(42)	1.174 (23)	P–O(2)	1.607 (13)
Ir(1)–C(12)	1.881 (16)	O(1)–C(1)	1.473 (20)	C(11)–O(11)	1.116 (21)
Ir(2)–Ir(3)	2.688 (1)	O(3)–C(3)	1.433 (23)	C(13)–O(13)	1.176 (24)
Ir(2)–C(21)	1.950 (23)	C(2)–C(4)	1.511 (28)	C(22)–O(22)	1.132 (23)
Ir(2)–C(23)	1.923 (20)	C(4)–C(5)	1.538 (25)	C(31)–O(31)	1.116 (22)
Ir(3)–P	2.234 (4)	Ir(1)–Ir(3)	2.701 (1)	C(41)–O(41)	1.133 (29)
Ir(3)–C(32)	1.899 (20)	Ir(1)–C(11)	1.927 (17)	C(43)–O(43)	1.147 (26)
Ir(4)–C(42)	1.899 (19)	Ir(1)–C(13)	1.900 (19)	O(2)–C(2)	1.471 (24)
P–O(1)	1.571 (13)	Ir(2)–Ir(4)	2.697 (1)	C(1)–C(4)	1.508 (24)
P–O(3)	1.594 (12)	Ir(2)–C(22)	1.925 (19)	C(3)–C(4)	1.482 (28)
C(12)–O(12)	1.161 (21)	Ir(3)–Ir(4)	2.687 (1)	C(5)–C(6)	1.491 (28)
C(21)–O(21)	1.116 (26)	Ir(3)–C(31)	1.924 (18)		
C(23)–O(23)	1.138 (25)	Ir(4)–C(41)	1.929 (24)		

Table 2 (cont.)

Ir(2)–Ir(1)–Ir(3)	59.9 (1)	Ir(2)–Ir(1)–Ir(4)	60.2 (1)
Ir(3)–Ir(1)–Ir(4)	59.8 (1)	Ir(2)–Ir(1)–C(11)	101.0 (4)
Ir(3)–Ir(1)–C(11)	101.4 (4)	Ir(4)–Ir(1)–C(11)	157.7 (4)
Ir(2)–Ir(1)–C(12)	152.0 (5)	Ir(3)–Ir(1)–C(12)	97.4 (5)
Ir(4)–Ir(1)–C(12)	95.1 (5)	C(11)–Ir(1)–C(12)	99.3 (7)
Ir(2)–Ir(1)–C(13)	94.3 (5)	Ir(3)–Ir(1)–C(13)	151.2 (5)
Ir(4)–Ir(1)–C(13)	97.6 (6)	C(11)–Ir(1)–C(13)	95.7 (7)
C(12)–Ir(1)–C(13)	102.6 (7)	Ir(1)–Ir(2)–Ir(3)	60.4 (1)
Ir(1)–Ir(2)–Ir(4)	60.0 (1)	Ir(3)–Ir(2)–Ir(4)	59.9 (1)
Ir(1)–Ir(2)–C(21)	93.7 (5)	Ir(3)–Ir(2)–C(21)	97.8 (5)
Ir(4)–Ir(2)–C(21)	151.0 (5)	Ir(1)–Ir(2)–C(22)	152.8 (6)
Ir(3)–Ir(2)–C(22)	94.5 (5)	Ir(4)–Ir(2)–C(22)	99.7 (6)
C(21)–Ir(2)–C(22)	100.3 (8)	Ir(1)–Ir(2)–C(23)	99.0 (6)
Ir(3)–Ir(2)–C(23)	154.1 (6)	Ir(4)–Ir(2)–C(23)	97.1 (7)
C(21)–Ir(2)–C(23)	99.2 (9)	C(22)–Ir(2)–C(23)	101.5 (8)
Ir(1)–Ir(3)–Ir(2)	59.7 (1)	Ir(1)–Ir(3)–Ir(4)	59.9 (1)
Ir(2)–Ir(3)–Ir(4)	60.2 (1)	Ir(1)–Ir(3)–P	106.2 (1)
Ir(2)–Ir(3)–P	98.5 (1)	Ir(4)–Ir(3)–P	158.0 (1)
Ir(1)–Ir(3)–C(31)	151.4 (5)	Ir(2)–Ir(3)–C(31)	97.6 (5)
Ir(4)–Ir(3)–C(31)	94.6 (5)	P–Ir(3)–C(31)	93.5 (5)
Ir(1)–Ir(3)–C(32)	97.7 (6)	Ir(2)–Ir(3)–C(32)	155.9 (6)
Ir(4)–Ir(3)–C(32)	102.7 (6)	P–Ir(3)–C(32)	95.8 (6)
C(31)–Ir(3)–C(32)	100.8 (8)	Ir(1)–Ir(4)–Ir(2)	59.7 (1)
Ir(1)–Ir(4)–Ir(3)	60.3 (1)	Ir(2)–Ir(4)–Ir(3)	59.9 (1)
Ir(1)–Ir(4)–C(41)	99.7 (7)	Ir(2)–Ir(4)–C(41)	153.6 (7)
Ir(3)–Ir(4)–C(41)	96.3 (7)	Ir(1)–Ir(4)–C(42)	151.6 (5)
Ir(2)–Ir(4)–C(42)	95.7 (6)	Ir(3)–Ir(4)–C(42)	96.2 (6)
C(41)–Ir(4)–C(42)	98.4 (8)	Ir(1)–Ir(4)–C(43)	96.6 (6)
Ir(2)–Ir(4)–C(43)	97.8 (6)	Ir(3)–Ir(4)–C(43)	153.2 (6)
C(41)–Ir(4)–C(43)	101.2 (9)	C(42)–Ir(4)–C(43)	101.1 (8)
Ir(3)–P–O(1)	119.0 (5)	Ir(3)–P–O(2)	115.1 (5)
O(1)–P–O(2)	101.7 (7)	Ir(3)–P–O(3)	114.6 (5)
O(1)–P–O(3)	103.0 (7)	O(2)–P–O(3)	101.0 (7)
Ir(1)–C(11)–O(11)	176.7 (15)	Ir(1)–C(12)–O(12)	178.5 (16)
Ir(1)–C(13)–O(13)	177.3 (17)	Ir(2)–C(21)–O(21)	176.6 (15)
Ir(2)–C(22)–O(22)	177.1 (18)	Ir(2)–C(23)–O(23)	173.6 (20)
Ir(3)–C(31)–O(31)	178.8 (14)	Ir(3)–C(32)–O(32)	177.0 (19)
Ir(4)–C(41)–O(41)	176.0 (20)	Ir(4)–C(42)–O(42)	177.6 (14)
Ir(4)–C(43)–O(43)	178.2 (16)	P–O(1)–C(1)	115.0 (10)
P–O(2)–C(2)	114.3 (12)	P–O(3)–C(3)	116.4 (12)
O(1)–C(1)–C(4)	111.5 (14)	O(2)–C(2)–C(4)	111.8 (16)
O(3)–C(3)–C(4)	111.8 (15)	C(1)–C(4)–C(2)	108.3 (15)
C(1)–C(4)–C(3)	107.5 (14)	C(2)–C(4)–C(3)	108.5 (17)
C(1)–C(4)–C(5)	110.4 (15)	C(2)–C(4)–C(5)	109.8 (15)
C(3)–C(4)–C(5)	112.2 (15)	C(4)–C(5)–C(6)	118.4 (17)

ligand occupies an axial position with respect to the Ir(1)–Ir(2)–Ir(3) plane, and the Ir(3)–P bond forms an angle of 74° with respect to this plane. The axial C(21)–Ir(3) and C(11)–Ir(3) bonds form corresponding angles of 82 and 77°, respectively. The Ir–C and C–O bond distances are in the normal range of values found for terminal CO groups. The Ir(3)–P distance (2.234(4) Å) is short with respect to all other Ir–P distances found in Ir_4 clusters which range from 2.28 to 2.36 Å [19] [23]. The $Ir(CO)_3$ and $Ir(CO)_2P$ moieties have

negligible differences in geometry. This is a logical consequence of the small *Tolman*'s angle [24] due to the small hindrance of this cyclic phosphite ligand. The $P(OCH_2)_3C$ cage has a non-crystallographic threefold axis passing through P, C(4) and C(5), and the C(6) atom is staggered with respect to C(1), C(2), and C(3).

We thank the *Swiss National Science Foundation* for financial support.

Experimental Part

1. *General.* See [17].

2. *Undecacarbonyltris(triphenyl phosphite)tetrairidium* ($[Ir_4(CO)_{11}\{P(OPh)_3\}]$, **1**), *Undecacarbonyltris(trimethyl phosphite)tetrairidium* ($[Ir_4(CO)_{11}\{P(OMe)_3\}]$, **2**), *and Undecacarbonyltris(4-ethyl-2,6,7-trioxa-1-phosphabicyclo[2.2.2]octane)tetrairidium* ($[Ir_4(CO)_{11}\{P(OCH_2)_3CEt\}]$, **3**). A soln. of (NEt_4) $[Ir_4(CO)_{11}I]$ (600 mg, 0.45 mmol), $P(OPh)_3$ (118 µl, 0.45 mmol), and $AgPF_6$ (114 mg, 0.45 mmol) in CH_2Cl_2 (150 ml) was stirred under N_2 at −20° for 30 min, then at r.t. for 2 h. After filtration of AgI, the yellow soln. was reduced in volume and submitted to prep. TLC (silica gel *Merck 60F-254*, 20 × 20 × 0.2 plate, CH_2Cl_2/hexane 1:3). The 1st fraction gave yellow crystals of **1** (431 mg, 69%) after recrystallization from CH_2Cl_2/heptane at −25°. A 2nd fraction contained the corresponding disubstituted product (5%). **1**: IR (CH_2Cl_2, 298 K): 2096*m*, 2059v*s*, 2039*s*, 2017*m*, 1856*w*. IR (nujol, 298 K): 2102*m*, 2055v*s*, 2035*s*, 2017*m*, 1974*m* (CO). $^{31}P\{^1H\}$-NMR (CD_2Cl_2; 85% H_3PO_4 as external ref.): at 173 K: 67.09 (**1A**), 50.39 (**1B**), rel. intensities 1:0.03; at 298 K: 1 signal at 57.83. ^{13}C-NMR (CD_2Cl_2, 173 K, CO region, rel. intensities in parentheses): 202.4 (0.06); 195.5 (0.03); 170.4 (0.03); 169.8 (0.06); 157.1 (2); 156.8 (*d*, $^1J(C,P) = 3.2$, 2); 155.5 (2); 154.4 (2); 153.8 (2.1); 153.3 (*d*, $^3J(C,P) = 58$, 1); 149.9 (*d*; < 0.1); signals of the 2 pairs of axial and apical CO's of **1B**, probably hidden under one or two of the main resonances. 2D-COSY (CD_2Cl_2, 188 K, $F_1 = 1385$ Hz): cross peaks with similar vicinal $^3J(CO,CO)$ (11 ± Hz) between δ 157.1/154.4 (*2* and *5*, resp.; see *Scheme*) and between δ 156.8 (*1*)/153.8 (*4*) of **1A**; thus, δ 155.5 (no coupling) is assigned to CO's *3* (see *Scheme*) and δ 153.3 to the unique CO *6* in pseudo-*trans*-position to P. 2D-NOESY (CD_2Cl_2, 193 K, $F_1 = 650.2$ Hz, mixing time 70 ms): cross peaks of 1st order between δ 155.5/156.8 (*d*) and 153.8; thus, the dynamic connectivity is $1 \leftrightarrow 3 \leftrightarrow 4$, corresponding to the merry-go-round responsible for the isomerisation $\mathbf{A} \rightleftarrows \mathbf{B}$ (k_1); a NOESY taken with a longer mixing time is similar to that observed for $[Ir_4(CO)_{11}(t\text{-BuNC})]$ (*Fig. 2b* in [17]); no exchange of CO *6* with other CO's. Anal. calc. for $C_{29}H_{15}Ir_4O_{14}P$ (1387.3): C 25.11, H 1.09, P 2.23; found: C 25.03, H 1.23, P 2.19.

The same procedure as for **1** starting with $P(OMe)_3$ (53 µl, 0.45 mmol) or $P(OCH_2)_3CEt$ (*Fluka*; 73 mg, 0.45 mmol) gave **2** (62%) and **3** (73%), resp.

2: IR (CH_2Cl_2, 298 K): 2091*m*, 2055v*s*, 2033*s*, 2022*s*, 1849*m*, 1833*m*. IR (nujol; 298 K): 2096*s*, 2055v*s*, 2039v*s*, 2023*s*, 2001*s* (CO). $^{31}P\{^1H\}$-NMR (CD_2Cl_2); at 173 K: 101.52 (**2C**), 79.34 (**2A**), 65.87 (**2B**), rel. intensities 0.01:0.48:1; at 298 K: 1 signal at 70.91. ^{13}C-NMR (CD_2Cl_2, 173 K, CO region): 204.2 (2); 203.9 (0.02); 197.0 (2); 173.1 (*d*, $J(C,P) = 9$, 1); 170.8 (< 0.1); 170.7 (2); 160.2 (*d*, $^1J(C,P) = 6$, 1); 157.7 (2); 157.6 (< 0.1); 156.2 (1.9); 155.1, 154.5, 154.3 (*d*, $^3J(C,P) = 45$, CO of **2B** pseudo-*trans* to P), 154.0, 153.9, 153.8 (all < 0.1, sun 3.4 ± 3); 152.4 (2). Anal. calc. for $C_{14}H_9Ir_4O_{14}P$ (1201.1): C 14.00, H 0.76, P 2.58; found: C 13.92, H 0.81, P 2.51.

3: IR (CH_2Cl_2, 298 K): 2094*m*, 2057v*s*, 2038*s*, 2015*s*, 1850*m*. IR (nujol, 298 K): 2095*s*, 2049v*s*, 2031v*s*, 2017*s*, 1988*m* (CO). $^{31}P\{^1H\}$-NMR (CD_2Cl_2): at 173 K: 86.28 (**3C**), 52.83 (**3A**), 50.05 (**3B**), rel. intensities 0.001:1:0.35; at 298 K: 1 signal at 54.73. ^{13}C-NMR (CD_2Cl_2, 173 K): 202.5 (0.7); 196.8 (0.35, μ_2-CO's of **3B**); 200.8, 196.6 (< 0.1 each, μ_2-CO's of **3C**); 172.3 (*d*, $^1J(C,P) = 9.2$, 0.4); 170.1 (0.7, radial CO's of **3B**); 170.3 (< 0.1); 159.0 (*d*, $^1J(C,P) = 6$, 2, CO's *1* of **3A**); 157.2 (0.7); 156.5 (< 0.1); 155.8, 155.2, 155.0, 154.6 (total 9.5); 153.3 (< 0.1); 152.3 (0.7). Anal. calc. for $C_{17}H_{11}Ir_4O_{14}P$ (1239.1): C 16.48, H 0.89, P 2.50; found: C 16.35, H 0.96, P 2.64.

3. *Crystal-Structure Determination.* A yellow crystal (0.10 × 0.10 × 0.07 mm) of **3** was sealed in a *Lindemann* glass capillary under N_2. Monoclinic, space group $P2_1/n$; $a = 9.004(2)$ Å, $b = 11.867(2)$ Å, $c = 24.254(4)$ Å, $\beta = 96.69(2)°$, $V = 2573.9(8)$ Å^3, $Z = 4$, $\mu = 20.742$ mm^{-1}. The diffraction intensities were collected at r.t. on a *Siemens-P4* diffractometer; MoK_α ($\lambda = 0.71073$ Å), graphite monochromatised, 2θ range = 2.0–50.0°, scan type 2θ–θ with a scan range of 2.00°; 8048 reflections collected, 4545 independent reflections ($R_{int} = 3.44\%$); 3098 observed reflections ($F > 4.0\ \sigma(F)$), semi-empirical absorption correction with min./max. transmission = 0.0085/0.0355. The quantity minimized was $\Sigma w (F_o - F_c)^2$ with $w^{-1} = \sigma^2(F) + 0.010\ F^2$; for the H-atoms the riding model with fixed isotropic U was used; 325 parameters were refined to final indices $R = 3.61\%$, $R_w = 4.23\%$ (for all data $R = 6.60\%$, $R_w = 5.29\%$): goodness-of-fit = 0.89, largest difference peak 1.44 e Å^{-3}, largest difference hole

-1.08 e Å^{-3}. The Ir-atoms were localized using direct methods and the remaining P-, O- and C-atoms were localized on the subsequent *Fourier* difference maps. The SHELXTL IRIS program package was used.

Supplementary Material. – Lists of the atomic fractional coordinates, equivalent isotropic thermal parameters observed and calculated structure factors, and anisotropic displacement coefficients are available from *R.R.* and are deposited with the *Cambridge Crystallographic Data Center*.

REFERENCES

[1] K.J. Karel, J.R. Norton, *J. Am. Chem. Soc.* **1974,** *96,* 6812.

[2] G.F. Stuntz, J.R. Shapley, *Inorg. Chem.* **1976,** *15,* 1994; *J. Am. Chem. Soc.* **1977,** *99,* 607.

[3] D.J. Darensbourg, M.J. Incorvia, *J. Organomet. Chem.* **1979,** *171,* 89; *Inorg. Chem.* **1980,** *19,* 2585; D.J. Darensbourg, B.J. Baldwin-Zuschke, *J. Am. Chem. Soc.* **1982,** *104,* 3906; D.J. Darensbourg, B.S. Peterson, R.E. Schmidt, Jr., *Organometallics* **1982,** *1,* 306.

[4] D.C. Sonnenberger, J.D. Atwood, *Inorg. Chem.* **1981,** *20,* 3243; *J. Am. Chem. Soc.* **1982,** *104,* 2113; *Organometallics* **1982,** *1,* 694.

[5] R.E. Benfield, B.F.G. Johnson, *J. Chem. Soc., Dalton Trans.* **1978,** 1554; B.F.G. Johnson, Y.V. Roberts, *Inorg. Chim. Acta* **1993,** *205,* 175.

[6] J-Q. Wang, J-K. Shen, Y-C. Gao, Q-Z. Shi, F. Basolo, *J. Organomet. Chem.* **1991,** *417,* 131.

[7] B.L. Booth, M.J. Else, R. Fields, R.N. Haszeldine, *J. Organomet. Chem.* **1971,** *27,* 119; N.M.J. Brodie, A.J. Poë, *ibid.* **1990,** *383,* 531; D. Labroue, R. Queau, R. Poilblanc, *ibid.* **1980,** *186,* 101.

[8] J.D. Atword, 'Inorganic and Organometallic Reaction Mechanisms', Brooks/Cole, Monterey, CA., 1985, p. 123.

[9] B.T. Heaton, L. Longhetti, L. Garlaschelli, U. Sartorelli, *J. Organomet. Chem.* **1980,** *192,* 431; B.T. Heaton, L. Strona, R. Della Pergola, L. Garlaschelli, U. Sartorelli, I.H. Sadler, *J. Chem. Soc., Dalton Trans.* **1983,** 173; D.T. Brown, T. Eguchi, B.T. Heaton, J.A. Iggo, R. Whyman, *ibid.* **1991,** 677.

[10] M.A. Cohen, D.R. Kidd, T.L. Brown, *J. Am. Chem. Soc.* **1975,** *97,* 4408.

[11] D.J. Darensbourg, M.J. Incorvia, *Inorg. Chem.* **1981,** *20,* 1911.

[12] B.T. Heaton, L. Longhetti, D.M.P. Mingos, C.E. Briant, P.C. Minshall, B.R.C. Theobald, L. Garlaschelli, U. Sartorelli, *J. Organomet. Chem.* **1981,** *213,* 333.

[13] B.E. Mann, C.M. Spencer, A.K. Smith, *J. Organomet. Chem.* **1983,** *244,* C17; B.E. Mann, B.T. Pickup, A.K. Smith, *J. Chem. Soc., Dalton Trans.* **1989,** 889.

[14] D. Braga, R. Ros, R. Roulet, *J. Organomet. Chem.* **1985,** *286,* C8; A. Strawczynski, R. Ros, R. Roulet, *Helv. Chim. Acta* **1988,** *71,* 867; A. Strawczynski, G. Suardi, R. Ros, R. Roulet, *ibid.* **1993,** submitted.

[15] M.J. Davis, R. Roulet, *Inorg. Chim. Acta* **1992,** *197,* 15.

[16] G.F. Stuntz, J.R. Shapley, *J. Organomet. Chem.* **1981,** *213,* 389.

[17] A. Orlandi, R. Ros, R. Roulet, *Helv. Chim. Acta* **1991,** *74,* 1464.

[18] G. Ciani, M. Manassero, V.G. Albano, F. Canziani, G. Giordano, S. Martinengo, P. Chini, *J. Organomet. Chem.* **1978,** *150,* C17.

[19] R. Ros, A. Scrivanti, V.G. Albano, D. Braga, L. Garlaschelli, *J. Chem. Soc., Dalton Trans.* **1986,** 2411.

[20] J.S. Leigh, Jr., *J. Magn. Reson.* **1971,** *4,* 308.

[21] A. Strawczynski, R. Ros, R. Roulet, *Helv. Chim. Acta* **1988,** *71,* 1885.

[22] R. Della Pergola, L. Garlaschelli, S. Martinengo, F. Demartin, M. Manassero, M. Sansoni, *Gazz. Chim. Ital.* **1987,** *117,* 245; M.R. Churchill, J.P. Hutchinson, *Inorg. Chem.* **1979,** *18,* 2451; G. Bondietti, R. Ros, R. Roulet, F. Musso, G. Gervasio, *Inorg. Chim. Acta* **1993,** in press.

[23] V.G. Albano, P.L. Bellon, V. Scatturin, *J. Chem. Soc., Chem. Commun.* **1967,** 730; A. Strawczynski, R. Ros, R. Roulet, D. Braga, C. Gradella, F. Grepioni, *Inorg. Chim. Acta* **1990,** *170,* 17; A.J. Blake, A.G. Osborne, *J. Organomet. Chem.* **1984,** *260,* 227; J.A. Clucas, M.M. Harding, B.S. Nicholis, A.K. Smith, *J. Chem. Soc., Chem. Commun.* **1984,** 319; D.J. Darensbourg, B.J. Baldwin-Zuschke, *Inorg. Chem.* **1981,** *20,* 3846; F. Demartin, M. Manassero, M. Sansoni, L. Garlaschelli, U. Sartorelli, *J. Organomet. Chem.* **1981,** *204,* C10.

[24] C.A. Tolman, *J. Am. Chem. Soc.* **1974,** *96,* 53; C.A. Tolman, *Chem. Rev.* **1977,** *77,* 313.